ISA Transactions xxx (xxxx) xxx

Contents lists available at ScienceDirect

ISA Transactions

journal homepage: www.elsevier.com/locate/isatrans

Research article

Adaptive hybrid intelligent MPPT controller to approximate effectual wind speed and optimal rotor speed of variable speed wind turbine

R. Sitharthan [a,*], Madurakavi Karthikeyan [a], D. Shanmuga Sundar [b], S. Rajasekaran [a]

[a] *School of Electrical & Electronics Engineering, Madanapalle Institute of Technology & Science, Madanapalle, Andhra Pradesh 517325, India*
[b] *Departamento de Física, Facultad de Ciencias Físicas y Matemáticas, Universidad de Chile, Santiago, Chile*

HIGHLIGHTS

- Modelling and control of the doubly fed induction generator based wind turbine.
- Optimal power extraction through developed hybrid intelligent controller.
- Rationalizing the pulse width modulation of back–back power electronic converter.

ARTICLE INFO

Article history:
Received 18 June 2018
Received in revised form 28 May 2019
Accepted 31 May 2019
Available online xxxx

Keywords:
Doubly-fed induction generator
Wind turbine
Maximum power point tracking
Particle swarm optimization
Radial basis function neural network

ABSTRACT

Operating wind power generation system at optimal power point is essential which is achieved by employing a Maximum Power Point Tracking (MPPT) control strategy. This literature focuses on developing a novel particle swarm optimization algorithm enhanced radial basis function neural network supported TSR based MPPT control strategy for Doubly Fed Induction Generator (DFIG) based wind power generation system. The proposed hybrid MPPT control strategy estimates the effective wind speed and estimates the optimal rotor speed of the wind power generation system to track the maximum power. The proposed controller extremely reduces the speed dissimilarity range of wind power generation system, which leads to rationalizing the pulse width inflection of DFIG rotor side converter. This in turn, increases the system's reliability and delivers an effective power tracking with reduced converter losses. Furthermore, by utilizing the proposed MPPT controller, the converter size can be reduced to 40%. Therefore, the overall cost of the system can be gradually decreased. To validate the performance of the proposed MPPT controller, an extensive simulation study has been carried out under medium and high wind speed conditions in MATLAB/Simulink. The obtained results have been justified using experimental analysis.

1. Introduction

Energy crisis, environmental pollution, and poor energy efficiency are the most important problems faced by the world in past decades. In-order to solve these issues and to fulfil the energy needs the power suppliers have started shifting to renewable energy-based power generation systems. [1]. Among various Renewable Energy Resources (RER), Wind Power Generation System (WPGS) is used most often known for its efficient power generation and advanced control strategy [2]. The WPGS is classified as Variable Speed Wind Turbine (VSWT) and Fixed Speed Wind Turbine (FSWT) based on their range of operation [3]. Among these, VSWT is often chosen for its improved energy production and reduced flickering effect [4]. Furthermore, the VSWT are generally operated with Doubly Fed Induction Generator (DFIG) or Permanent Magnet Synchronous Generator (PMSG). Among these generators, DFIG is preferred often for its extreme quality to function in all quadrants for achieving active and reactive power formation throughout the grid integration [5]. Moreover, by using DFIG the fabrication cost and losses with respect to power electronic converter are reduced when compared to the other generators [6].

It is necessary to extract as much power as possible from the wind. Therefore, Maximum Power Point Technique (MPPT) is employed to extract maximum available power from the wind. In [7–13], several MPPT control strategies were discussed to extract maximum power. The most profuse and popular techniques include; Tip Speed Ratio (TSR) [14,15], Power Signal Feedback (PSF) [16,17], Hill–Climb Searching (HCS) [18,19], Optimal Torque Control (OTC) [20,21] and Perturb and Observer (PO) [22] methods. These methods use different control topologies for their effective extraction of maximum power. But, these methods perform effectively only when there are no rapid wind speed

---

* Corresponding author.
E-mail address: sithukky@gmail.com (R. Sitharthan).

https://doi.org/10.1016/j.isatra.2019.05.029

Please cite this article as: R. Sitharthan, M. Karthikeyan, D.S. Sundar et al., Adaptive hybrid intelligent MPPT controller to approximate effectual wind speed and optimal rotor speed of variable speed wind turbine. ISA Transactions (2019), https://doi.org/10.1016/j.isatra.2019.05.029.

variations and have potential barriers to uncertain wind flow. The MPPT methodologies are classified into two types, one is sensor-based wind speed estimation MPPT topology and the other type is MPPT topology to estimate wind speed without sensor. The MPPT topology with sensor is normally used in conventional WPGS and it increases the cost of WPGS and decreases the reliability incase of inaccurate measuring of wind speed. Hence, this MPPT topology is not preferred in present wind turbine design. Recently, research efforts are very much focused on developing sensor less wind speed estimation based TSR MPPT controller. The sensor less control strategy has the capability to function with measured parameters without the knowledge of wind speed and turbine parameters.

Meantime, the conventional controllers are being replaced by the Artificial Neural Network (ANN) controllers. The ANN is identical in exhibiting complex nonlinear systems [23]. In [24] a multilayer perceptron ANN has been designed to find the wind speed without sensor. The system has been trained for the different number of nodes in the hidden layer. The developed system has an ability to forecast the wind speed based on haulage parameters [20]. The hybrid intelligent techniques have been implemented as they apprehend the non-linear relationships between input/output data and shows an appropriate estimation of wind speed rather than the simple intelligent technique [22–32]. Thus, it is most essential to develop a hybrid intelligent control strategy that effectively performs in both constant as well as in variable wind speed conditions.

In this literature, a novel hybrid intelligent technique to extract maximum available power from the wind through wind turbine is being proposed. The proposed MPPT approach uses TSR control strategy along with Radial Basis Function Neural Network supervised by Modified Particle Swarm Optimization based hybrid intelligent controller (RBFNN-MPSO). The RBFNN is trained using gradient descent algorithm and to increase the learning capability of the training process (adjusting the network's learning rate) the MPSO algorithm is implemented. The proposed hybrid RBFNN-MPSO based MPPT controller is developed to obtain maximum output power as well as effective estimation of wind speed. The proposed hybrid RBFNN-MPSO based MPPT control strategy estimates effectual wind speed and optimal rotor speed of WPGS to track the maximum power above and below the rated speed of wind turbine. Furthermore, the proposed MPPT controller extremely reduces the speed dissimilarity range of WPGS and thereby leads to rationalize the pulse width modulation of back–back power electronic converter. Furthermore, it also increases the system's reliability and effective power tracking with reduced converter losses. The performance of the proposed method has been demonstrated through MATLAB/Simulink simulation studies and validated through experimental investigation.

2. WPGS modelling and description

The aerodynamic turbine and DFIG are interconnected to each other through a gear shaft system. The WPGS generates an electrical power (*Pe*) by transforming the wind power (*Pw*) into mechanical power (*Pm*) and generated *Pe* is being directly fed into the grid system through converters.

2.1. Wind turbine modelling

The aerodynamic power is converted into mechanical power by means of the wind turbine. The mechanical power produced by a wind turbine is given by [1–6],

$$P_m = \frac{1}{2}\rho C_p(\lambda, \beta) A W^3 \tag{1}$$

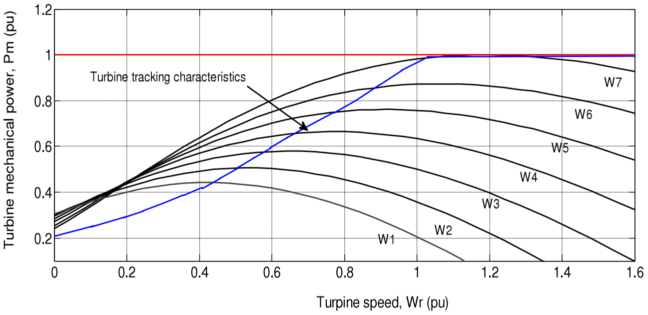

Fig. 1. Wind turbine characteristics curve.

where, W is the variable wind speed, A is the blade swept area, ρ is the air density, C_p is the power coefficient, λ is the tip speed ratio and β is the pitch angle. The power co-efficient maximization of the turbine system depends on the function (λ, β). The tip speed ratio of the wind turbine is given by,

$$\lambda = \frac{\omega_r^* R}{W} \tag{2}$$

where, ω_r is the rotor rotational speed and R is the radius of the turbine blades swept, respectively. In this analysis the pitch angle of the system is set to zero to yield maximum power and the coefficient function $Cp\ (\lambda, \beta)$ is given by,

$$C_p(\lambda, \beta) = 0.0066\lambda + 0.52e^{-\frac{21}{\lambda_j}}\left(-0.4\beta - 5 + \frac{116}{\lambda_j}\right) \tag{3}$$

Fig. 1 shows the characteristic of the turbine speed with respect to turbine mechanical power. The optimum rotor speed ω_{opt} can be achieved during maximal wind speed at certain range of rotor speed and this specific speed is related to optimum tip speed ratio λ_{opt} and the turbine can extract maximum power when maintained at λ_{opt} [14–17]. The maximum power can be achieved only at the optimum speed of rotation which can be obtained through controlling the rational speed of the turbine [18].

2.2. Doubly fed induction generator modelling

The dynamic voltage and flux equations in an arbitrary *d-q* reference frame of the investigated DFIG in the literature has been developed by applying Concordia and Park's transformation and is given by [33–35],

$$V_{ds} = \frac{d\phi_{ds}}{dt} - \omega_s\phi_{qs} + Rl_s il_{ds} \tag{4}$$

$$V_{qs} = \frac{d\phi_{qs}}{dt} + \omega_s\phi_{ds} + Rl_s il_{qs} \tag{5}$$

$$V_{dr} = \frac{d\phi_{dr}}{dt} - \omega_r\phi_{qr} + Rl_r il_{dr} \tag{6}$$

$$V_{qr} = \frac{d\phi_{qr}}{dt} + \omega_r\phi_{dr} + Rl_r il_{qr} \tag{7}$$

where $R1_s$ and $R1_r$ represents the rotor and stator winding respectively. The rotational speed is given by ω_r and the speed in synchronous reference frame is represented as ω_s. Therefore, the slip frequency is represented as $s\omega_{s=}\omega_s$ - ω_r. The flux linkages of the DFIG system are given by,

$$\varphi_{ds} = Lk_s i_{ds} + Lk_m i_{dr} \tag{8}$$

$$\varphi_{qs} = Lk_s i_{qs} + Lk_m i_{qr} \tag{9}$$

$$\varphi_{dr} = Lk_m i_{ds} + Lk_r i_{dr} \tag{10}$$

$$\varphi_{qr} = Lk_m i_{qs} + Lk_r i_{qr} \tag{11}$$

Please cite this article as: R. Sitharthan, M. Karthikeyan, D.S. Sundar et al., Adaptive hybrid intelligent MPPT controller to approximate effectual wind speed and optimal rotor speed of variable speed wind turbine. ISA Transactions (2019), https://doi.org/10.1016/j.isatra.2019.05.029.

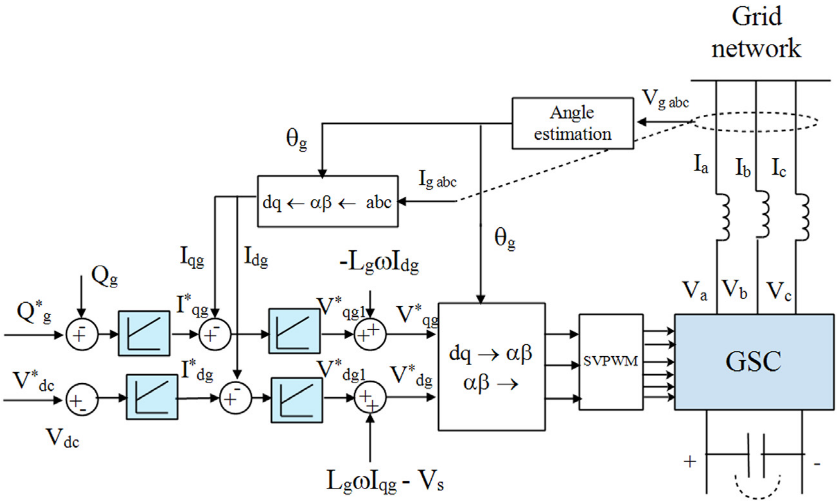

Fig. 2. Grid side converter control strategy.

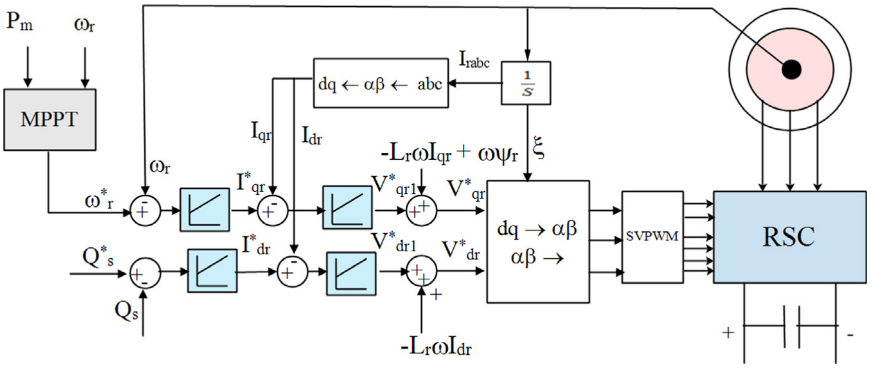

Fig. 3. Rotor side converter control strategy.

where Lk_s, Lk_r, and Lk_m are the stator leakage, rotor leakage and mutual inductance respectively. The DFIG system corresponding electromagnetic torque is given as,

$$T_e = Lk_m(i_{qs}i_{dr} - i_{ds}i_{qr}) \tag{12}$$

By neglecting the power loss of stator resistance, the corresponding stator real and reactive power is given as [33],

$$P_e = \frac{3}{2}(V_{ds}i_{ds} + V_{qs}i_{qs}) \tag{13}$$

$$Q_e = \frac{3}{2}(V_{qs}i_{ds} + V_{ds}i_{qs}) \tag{14}$$

Further, the typical parameters of the DFIG system considered in this analysis are taken in per unit (p.u.) and the parameters value of stator and rotor resistance, leakage inductance and magnetizing inductance for the studied 2.5 MW DFIG system are given in Appendix.

3. DFIG converter control strategy

This section briefly describes about the designing and implementing of control systems for DFIG based WPGS. When considering the control aspect of the WPGS, the converter controller plays a vital role and is classified as, (i) grid side converter and (ii) rotor side converter control system. The DFIG based WPGS modelled for the study consists of back-to-back VSC and is equipped with insulated bipolar gate transistors.

3.1. Grid side converter control system

The grid side converter power flow is controlled consecutively to keep the dc-link voltage at its nominal voltage. The converter in the grid side is controlled by vector logic in grid voltage reference frame. The output power is regulated to maintain the dc-link voltage at the constant value. The grid voltage vector can be obtained by identifying the correlation of *q*-axis of the rotor reference frame to the grid voltage and it is given by,

$$V = V_d + 0j \tag{15}$$

At the position $V_d = 0$, the real and reactive power of the DFIG system is given as,

$$P_e = \frac{3}{2}(V_q i_q) \tag{16}$$

$$Q_e = \frac{3}{2}(V_q i_d) \tag{17}$$

Fig. 2 shows the block diagram of grid side converter control scheme. The required real and reactive power can be obtained by controlling *d*-*q* current components. Two control loops are used in GSC to control the real and reactive powers. They are outer voltage controller and inner current controller. The *d*-axis voltage control loop sets the current reference for controlling active power respectively. The power flow from DC-link to grid can be controlled by *d*-axis current controller to maintain the dc-link voltage as constant value. The *q*-axis voltage control loop can set the current reference for controlling reactive power respectively.

Please cite this article as: R. Sitharthan, M. Karthikeyan, D.S. Sundar et al., Adaptive hybrid intelligent MPPT controller to approximate effectual wind speed and optimal rotor speed of variable speed wind turbine. ISA Transactions (2019), https://doi.org/10.1016/j.isatra.2019.05.029.

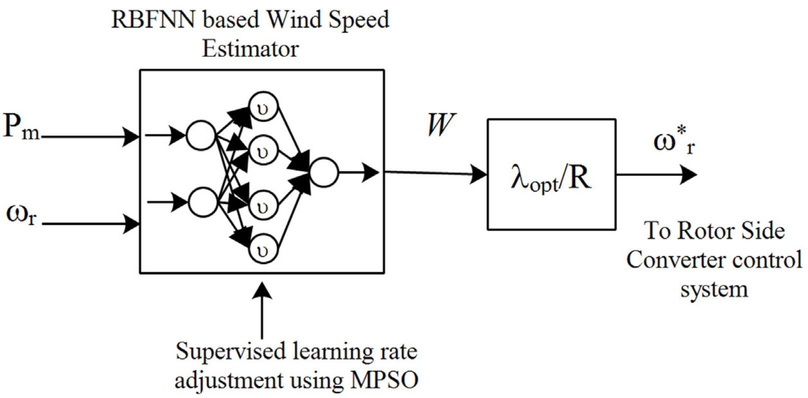

Fig. 4. Proposed hybrid RBFNN-MPSO based MPPT controller.

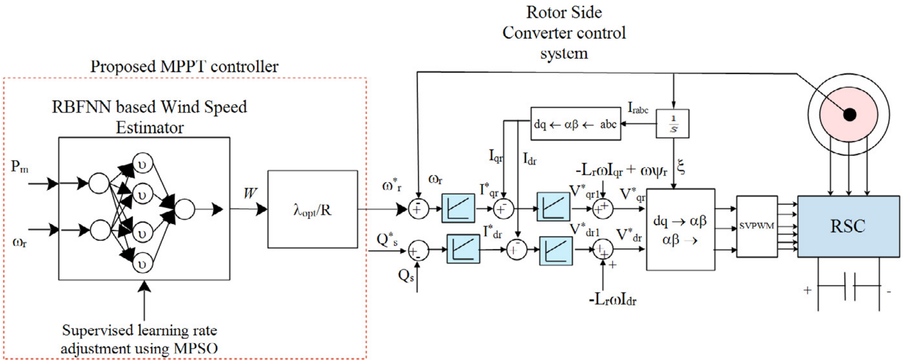

Fig. 5. Proposed intelligent MPPT control strategy.

In-order to control the reactive power, the value of the quadrature current reference should be set to zero in *q*-axis current control loop. Both *d*-axis and *q*-axis current control loop provides a voltage reference for the grid side inverter. That voltage reference can be compensated by adding rotational EMF recompense terms to the voltage vector component has been attained from the current controller using the following equations.

$$V_{dg} = L_g \omega i_{qg} + V_s \tag{18}$$

$$V_{qg} = -L_g \omega i_{dg} \tag{19}$$

The *d*-axis and *q*-axis reference voltages of the controller has been converted from coordinate to the stationary reference frame. These stationary reference signals are used to stimulate switching signals for grid side converter of DFIG-WPGS using pulse width modulation technique.

3.2. Rotor side converter control system

The Rotor Side Converter (RSC) control strategy has been shown in Fig. 3. The vector control logic is employed for controlling the rotor flux-oriented reference frame. In the proposed MPPT controller, the reference speed $\omega_r{}^*$ is defined as the command speed signal for the rotor side converter speed control loop. The electromagnetic torque can be controlled by adjusting rotational speed and thereby maximum power is tracked by the WPGS [23,25]. The system uses PI-type speed controller and the controller loop generates *q*-axis and *d*-axis current component, respectively. By regulating the *q*-axis component i_{qr} the rotor speed and torque can be controlled. Whereas, by regulating the *d*-axis component i_{dr} the stator reactive power can be controlled. These *d*-*q* components are possessed by PI-type current control loop and voltage component V_{dr} and V_{qr} are obtained. Further, to have forced dynamic control $V^*{}_{dr}$ and $V^*{}_{qr}$ are added with voltage vector components V_{dr} and V_{qr}. The V_{dr} and V_{qr} of the rotor side converter strategy is given as,

$$V_{dr} = V_r i_{dr} - R_r i_{dr} + \frac{L_r k d i_{dr}}{d_t} - \omega_r L_r k \, i_{qr} \tag{20}$$

$$V_{qr} = V_r i_{qr} - R_r i_{qr} + \frac{L_r k_r d i_{qr}}{d_t} + \omega_r L_r k_r i_{dr} \tag{21}$$

where L_r and R_r represents inductance and resistance of the rotor winding. V_r represents the voltage component of the rotor circuit, i_{dr} and i_{qr} denotes the current components of the rotor circuit. The *d*-axis and *q*-axis voltage command is fed to the pulse width modulator to generate appropriate switching pulses to the RSC.

4. Proposed sensor-less MPPT controller

A sensor-less wind speed approximation based TSR control is modelled in-order to extract the maximum power from the WPGS. The wind speed is approximated by RBFNN using the WPGS parameter P_m and ω_r as shown in Fig. 4. where, Pm is the mechanical power of WPGS obtained using Eq. (22).

$$P_m = \omega_r \left(J \frac{d\omega_r}{dt} \right) + P_e \tag{22}$$

where J is the moment of inertia of the rotor.

Whenever high wind gust flows and attains the rated speed of the turbine. The power gets maximized at certain rotor speed. That corresponding rotor speed is called an optimal rotational speed $\omega^*{}_r$ and the corresponding tip speed ratio is called an optimum tip speed ratio λ_{opt}. It is necessary to maintain the turbine at λ_{opt} to extract maximum available power from wind flow. This is possible through fine controlling the rotor speed dynamically and setting it at optimal value. Furthermore, using

Please cite this article as: R. Sitharthan, M. Karthikeyan, D.S. Sundar et al., Adaptive hybrid intelligent MPPT controller to approximate effectual wind speed and optimal rotor speed of variable speed wind turbine. ISA Transactions (2019), https://doi.org/10.1016/j.isatra.2019.05.029.

the approximated wind speed and knowledge of λ_{opt} the TSR control estimates the optimal reference rotor speed $\omega^{*}{}_{r}$.

The reference rotor speed $\omega^{*}{}_{r}$ is fed to the speed control loop of RSC control system as shown in Fig. 5. The figure shows the control strategy of the proposed intelligent MPPT control strategy. The estimated $\omega^{*}{}_{r}$ obtained from the MPPT controller has been fed as an input to the speed control loop of RSC. The function of RSC control strategy is discussed in Section 3.2. Consequently, when the wind flow is above the rated value of a turbine, the proposed MPPT controller normalizes the rotational speed of the generator to maintain the optimal TSR. In this case maximum power can be extracted. On the other hand, when the wind speed is below the rated speed, then the forecasted output power regulates the proposed MPPT controller to attain the reference speed. Thus, the optimal TSR is maintained and maximum power is extracted in the wind turbine. Through the proposed MPPT controller the speed variation range of wind generator is reduced. This leads to rationalizing the back to back converter pulse width modulation and reliability is improved with fewer converter losses.

4.1. Design of MPSO-RBFNN based MPPT

The architecture of the developed RBFNN for MPPT controller consists of the input layer (*i layer*), the hidden layer (*j layer*), and the output layer (*k layer*) is shown in Fig. 6. The wind speed W is estimated through NN by processing Pm and ω_{r} as the inputs. In this training process, totally 20,000 data have been used. Out of which 13,000 data have been used for training NN and 7000 data's have been used for testing NN. In this developed RBFNN, there are 2 neurons in the *i layer,* 14 neurons in the *j layer* and 1 neuron in the *k layer.* The performance goal set is maintained at $1e^{-04}$ and to increase the convergence the spread count is set at 3. In the developed neural network $i^{*}{}_{z}$ is the control function and the linearization of WPGS to apply the RBFNN controller is discussed and the basic layer function is given as follows [27–31].

(i) Layer 1 is defined as the input layer (*i layer*) and the node in this layer transmits the input right away to the hidden layer. The output transmitted is given as,

$$y_i^{(1)}(m) = f_i^{(1)}(net_i^{(1)}(m)) \qquad i = 1 \tag{23}$$

Such that, $net_i^{(1)}(m) = x_i^{(1)}(m)$ and m symbolize the nth iteration. $x_i^{(1)}(m)$ is the input and $y_i^{(1)}(m)$ is the output of input layer.

(ii) Layer 2 is defined as the hidden layer of the network with gaussian function as the membership function,

$$y_j^{(2)}(m) = S(net_j^{(2)}(m)), \qquad j = 1, 2, \ldots, 9 \tag{24}$$

where, sigmoid function of the network is given as $S(x) = {}^{1}/{}_{1+e^{-x}}$. Consequently, $y_i^{(1)}(m)$ is the input and $y_j^{(2)}(m)$ is the output of hidden layer. Further, the weights of the successive hidden layer and the input layers are connected by w_{ji}

(iii) Layer 3 generally denotes the final output of the number of layers present in the set of hidden and the input layers. The output layer is signified as,

$$O_{yk}^{(3)}(m) = f_k^{(3)}(net_k^{(3)}(g)) = W \tag{25}$$

where, $net_k^{(3)}(g) = i_z^{*}$, and $net_k^{(3)}(g)$ is given as,

$$net_k^{(3)}(g) = \sum_j w_{jk} \times x_j^{(2)}(n) \tag{26}$$

$O_{yk}^{(3)}(g)$ is the final output obtained from the neural network of the proposed controller. w_{kj} acts as the weights connecting the neurons from hidden layer to output layer.

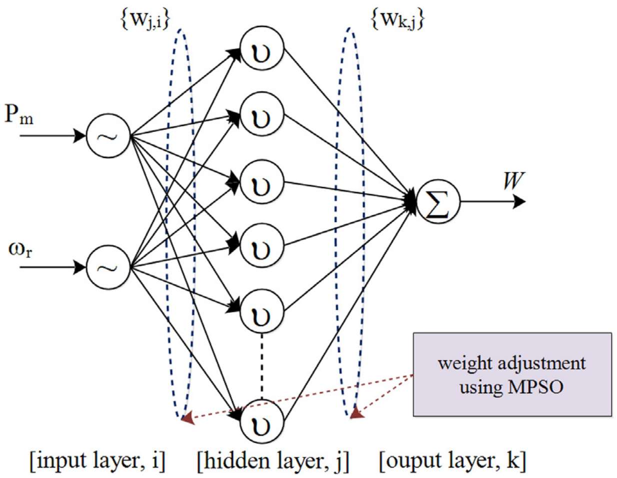

Fig. 6. Architecture of RBFNN.

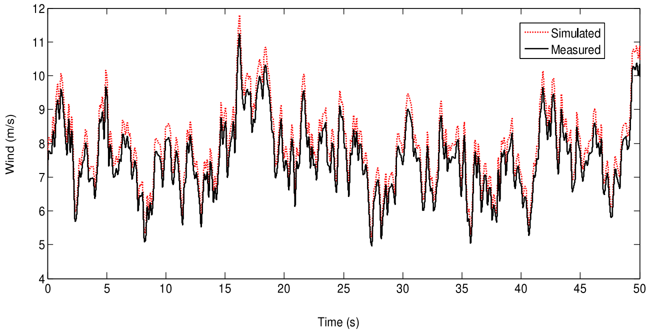

Fig. 7. Simulated moderate wind flow used in the study.

4.2. Controlled learning and training process

Whenever RBFNN becomes activated, the gradient descent based learning methodology has been employed to train the system. The erudition process has a capability to adjust RBFNN parameters through a specific learning pattern. The objective of learning process is to minimize the total error by placing the appropriate weight function to the connecting weights w_{ji} and w_{kj}. The error of the training progress is given by E and is expressed as,

$$E = \frac{1}{2}(p_m - \omega_r) = \frac{1}{2}e^2 \tag{27}$$

the training and testing of the neural network use specific learning pattern called chain rules. The rules of the process are described as follows,

Rule 1: revise the weights of w_{kj} in *layer k*.

The error term circulated is specified as,

$$\delta_k = -\frac{dE}{dnet_k^{(3)}} = \left[-\frac{dE}{dy_k^{(3)}}\frac{dy_k^{(3)}}{dnet_k^{(3)}}\right] \tag{28}$$

Therefore, the weight w_{kj} is rationalized as

$$\Delta w_{kj} = -\frac{dE}{dw_{kj}} = \left[-\frac{dE}{dy_k^{(3)}}\frac{dy_k^{(3)}}{dnet_k^{(3)}}\right]\left(\frac{dnet_k^{(3)}}{dw_{kj}}\right) = \delta_l y_j^{(2)} \tag{29}$$

and then rationalized Wight is specified as,

$$w_{kj}(m+1) = w_{kj}(m) + \xi_1 \Delta w_{kj} \tag{30}$$

Please cite this article as: R. Sitharthan, M. Karthikeyan, D.S. Sundar et al., Adaptive hybrid intelligent MPPT controller to approximate effectual wind speed and optimal rotor speed of variable speed wind turbine. ISA Transactions (2019), https://doi.org/10.1016/j.isatra.2019.05.029.

where ξ_1 represent the training rate adjustment of the *layer k*.

Rule 2: update the weights of w_{ji} in *layer j*

Through the help of training pattern, the weight w_{ji} is accustomed and is given as,

$$\Delta w_{ji} = -\frac{dE}{dw_{ji}} = \left[-\frac{dE}{dy_k^{(3)}}\frac{dy_k^{(3)}}{dnet_k^{(3)}}\right]\left(\frac{dnet_k^{(3)}}{dy_j^{(2)}}\frac{dy_j^{(2)}}{dw_{ji}}\right) \tag{31}$$

$$\Delta w_{ji} = \delta_k w w_{kj} y_j^{(2)}[1-y_j^{(2)}]x_i^{(1)} \tag{32}$$

Therefore, the connecting weight w_{ij} is updated as

$$w_{ji}(m+1) = w_{ji}(m) + \xi_2 \Delta w_{ji} \tag{33}$$

where ξ_2 represents the training rate adjustment of *layer j* and learning algorithm derives E till performance goal is reached.

4.2.1. Learning rate adjustment using MPSO

The learning rate adjustment has been carried out by MPSO algorithm and the training process is offline. MPSO find its optimal solution based on their existing population particles. Moreover, each surviving population signifies a hopeful solution to the problem. In this study, the MPSO is used for modifying the learning rates ξ_1 & ξ_2 of RBFNN. The function of MPSO for adjusting the RBFNN learning rates are explained in the following sections.

Step 1: Significant primary conditions

The initial step of the training set is to describe the basic parameter, which in turn optimized between maximum and minimum ranges. The study finds cohort particles to be $L_i^d = [L_i^1, L_i^2]$, where, L_i^1 & L_i^2 are the cohort particles for the RBFNN and their corresponding learning rates are γ_1 & γ_2. In this learning process, size of the population is set as p = 500 and particles dimension is to be d = 1 and the iteration is set as 1000.

Step 2: Adjusting random position & velocity

In the secondary stage of process, the initial position $P_i^d(N)$ and velocity $v_i^d(N)$ of all population are picked on arbitrary basis. Preliminary *pbest* of the particle is chosen based on its current position. Finally, *pbest* group are formed by best population using Rowlett wheel selection methodology. The preliminary value of $L_i^d(N)$ are engendered randomly as,

$$P_i^d \sim U[\gamma_{\min}^d, \gamma_{\max}^d] \tag{34}$$

$\gamma_{\min}^d, \gamma_{\max}^d$ represents the minimum and maximum bound of the training rates and $U[\gamma_{\min}^d, \gamma_{\max}^d]$ positions for the unvarying random variable outcome.

Step 3: Velocity Updating

In every step of iteration, the particle velocity is been restructured using the Eqs. (35) and (36). In this step, the two different obtained pseudorandom sequences $r_1 \sim U(0,1)$ and $r_2 \sim U(0,1)$ have been familiarized to model the stochastic nature of the algorithm [36–38]. For each dimension d, let P_i^d, $pbest_i^d$ be the current position and current personal *pbest* position. Then the reorganized velocity law is given as,

$$v_i^d(M+1) = v_i^d(M) + c_1 \cdot r_1 \cdot (pbest_i^d - P_i^d(M)) + c_2 \cdot r_2 \cdot (gbest_i^d - P_i^d(M)) \tag{35}$$

Step 4: Position updating

The new velocity takes care of position updating, at each step the current velocity is updated to the current position of the particle.

$$P_i^d(M+1) = P_i^d(M) + v_i^d(M+1) \qquad i = 1, \ldots, \text{p} \tag{36}$$

Step 5: Update pbests

When the new particle position is not disruption with reverence to the *gbest* particles, then the overwhelmed function of the particle can be analysed using the fitness function equation (37). The fitness function of each particle is derived as,

$$FIT = \frac{1}{0.1 + abs(\omega_r^* - \omega_r) * abs(p_m^* - p_m)} \tag{37}$$

Step 6: Update gbests

As the training phase of the algorithm, the fast merging of the *gbest* between the various values has been chosen as $pbest_i^d = [pbest_1^d, pbest_2^d, \ldots\ldots\ldots, pbest_p^d]$ which have the maximum fitness values.

Step 7: Convergence check

The ultimate goal of the algorithm is to reach the best and precise fitness particle for accomplishing the best fitness function. The best fitness function has been obtained by iterating the steps 3–6. The final highest $gbest_i^d$ is the optimal learning rate γ_1 *and* γ_2 of the RBFNN. The convergence point of the MPSO is controlled by the inertia weight *w* [29]. Minimum value of convergence is attained only at local optima. Highest values cannot cause the best convergence. The *w* can set with the help of following equation.

$$w = w_{\max} - \frac{w_{\max} - w_{\min}}{i_{x,\max}} i_x \tag{38}$$

where, i_x represents current iteration and $i_{x,max}$ represents maximum number of iterations.

5. Result and discussion

The performance and effectiveness of the hybrid RBFNN-MPSO based MPPT control strategy is assessed through the simulation study and validated through the experimental analysis. The proposed hybrid RBFNN-MPSO based MPPT controller along with the DFIG is simulated in the MATLAB/Simulink environment. The parameters used for the simulation study is listed in Appendix. To appraise the performance of the proposed hybrid RBFNN-MPSO based MPPT controller, the obtained results has been compared with existing technique [20,22,25] and [26]. Furthermore, to prove the robustness of the proposed controller the simulation study has been carried under two conditions, (i) Moderate wind speed and, (ii) High turbulence wind speed. The wind speed used in the study has been simulated based on the consolidated real time wind data recorded during months of June to July in Aralvaimozhi site, Tamilnadu, India.

5.1. Response of DFIG-WPGS with proposed MPPT control strategy for moderate wind speed

Initially the study has been carried out with moderate wind speed as shown in Fig. 7. In wind speed simulation, the tracking wind speed varies between 5 m/s to 12 m/s. The rated wind speed considered is 8 m/s. When the rated speed hits the wind turbine the WPGS starts converting the aerodynamic power into electrical power. The response obtained by the DFIG-WPGS with the hybrid RBFNN-MPSO based MPPT controller and hybrid ENN-MPSO based MPPT controller is depicted in Fig. 8. To reveal the effectiveness of the RBFNN-MPSO based MPPT controller, the obtained results is compared with the ENN-MPSO based MPPT controller throughout the studies. Fig. 8(a) depicts the DFIG's rotor speed and it can be clearly seen that the tracking error is found to be less than 2% for proposed MPPT controller. The results obviously specify a slower dynamic variation of the rotor speed in the RBFNN-MPSO based MPPT when compared to the ENN-MPSO based MPPT. Furthermore, with the proposed RBFNN-MPSO based MPPT strategy, the slip has been reduced to 40%.

Please cite this article as: R. Sitharthan, M. Karthikeyan, D.S. Sundar et al., Adaptive hybrid intelligent MPPT controller to approximate effectual wind speed and optimal rotor speed of variable speed wind turbine. ISA Transactions (2019), https://doi.org/10.1016/j.isatra.2019.05.029.

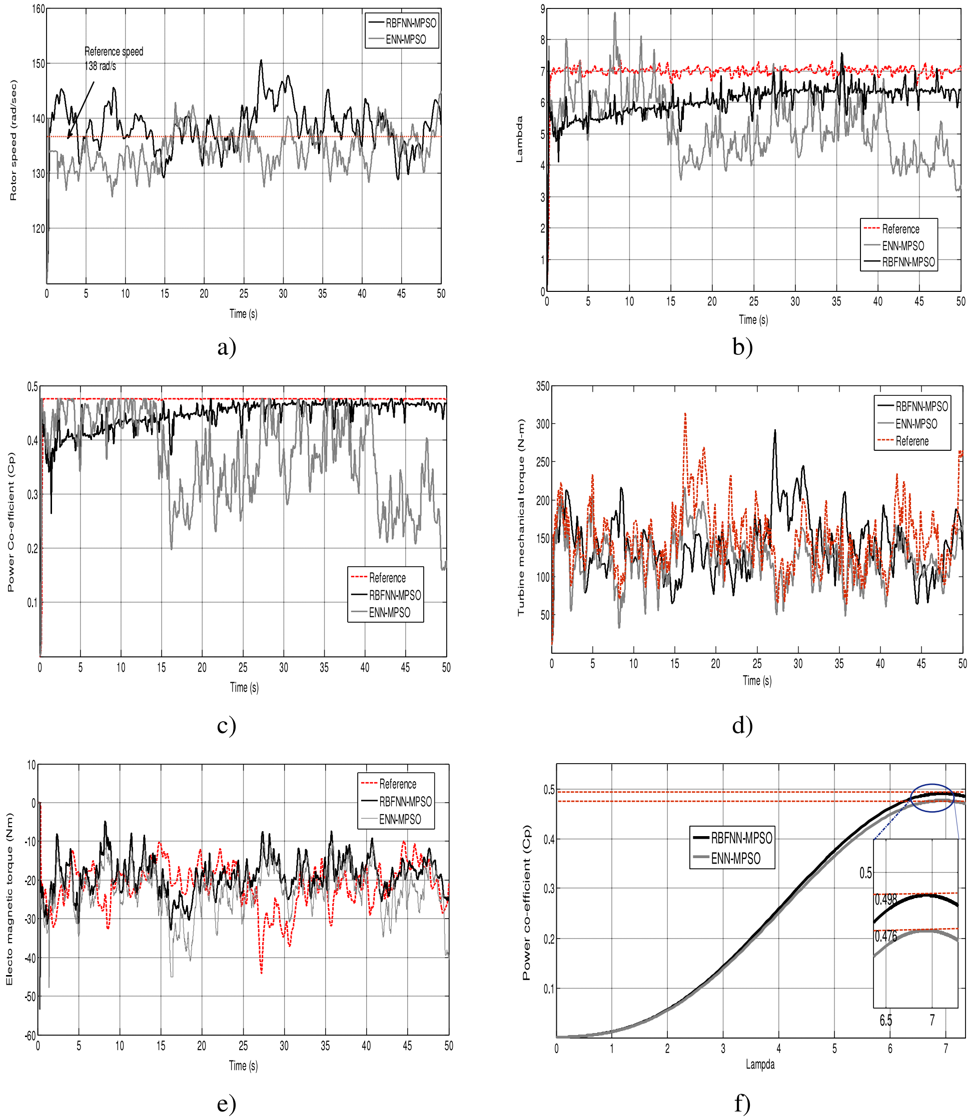

a) b) c) d) e) f)

Fig. 8. Obtained response of the DFIG-WPGS with MPPT controller for wind speed 5 m/s to 12 m/s. (a) Rotor speed (ω_r); (b) Tip speed ratio *(λ-Lambda)*; (c) Power co-efficient *(C_p)*; (d) Mechanical torque *(T_m)*; (e) Electromagnetic toque *(T_e)*; (f) MPPT-curve *(λ VsC_p)*.

Hence, slip is proportional to size of power converters, thereby the size of the converter can be reduced. Fig. 8(b) depicts the tip speed ratio of the WPGS and it can be observed that the proposed RBFNN-MPSO based MPPT maintains an optimal tip speed ratio nearly tracking the optimal tip speed ratio when compared to the ENN-MPSO MPPT strategy. The corresponding power coefficient obtained is depicted in Fig. 8(c). The RBFNN-MPSO based MPPT strategy tracks an optimal power with less oscillation than that of ENN-MPSO MPPT strategy. The turbine mechanical torque and DFIG electromagnetic torque is depicted in Fig. 8(d) and (e). Thus, it can be concluded that both strategies has an effective interaction with the rotor torque. Fig. 8(f) depicts the MPPT curve plotted between λ and C_p and it can be noted that for different wind speeds and at particular rotor speed the power coefficient is maximum. Also, it can be observed that the proposed RBFNN-MPSO based MPPT strategy achieves maximum power co-efficient of 0.498 and ENN-MPSO based MPPT strategy achieves power coefficient of 0.476 at optimal tip speed ratio, $\lambda = 6.8$. The optimal power obtained in RBFNN-MPSO based MPPT strategy is 2% higher when compared to ENN-MPSO MPPT strategy. Fig. 9 depicts the real power obtained by the DFIG-WPGS for 5 m/s to 11 m/s wind speeds.

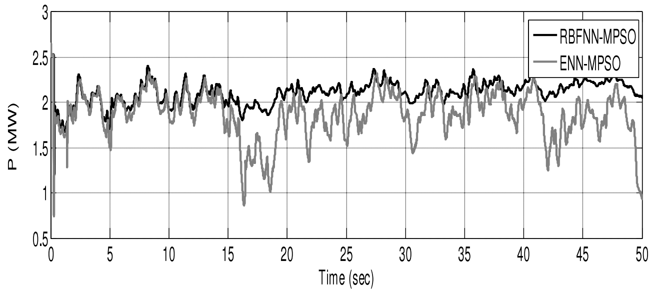

Fig. 9. Measured real power of DFIG-WPGS.

5.2. Response of DFIG-WPGS with proposed MPPT control strategy for high turbulence wind speed

To verify the performance of the proposed controller at dreadful condition a study has been carried out with high turbulence aerodynamic power. The wind speed considered for the study has been shown in Fig. 10. In wind speed simulation, the wind speed tracking varies between 14 m/s to 22 m/s. The rated wind speed

Please cite this article as: R. Sitharthan, M. Karthikeyan, D.S. Sundar et al., Adaptive hybrid intelligent MPPT controller to approximate effectual wind speed and optimal rotor speed of variable speed wind turbine. ISA Transactions (2019), https://doi.org/10.1016/j.isatra.2019.05.029.

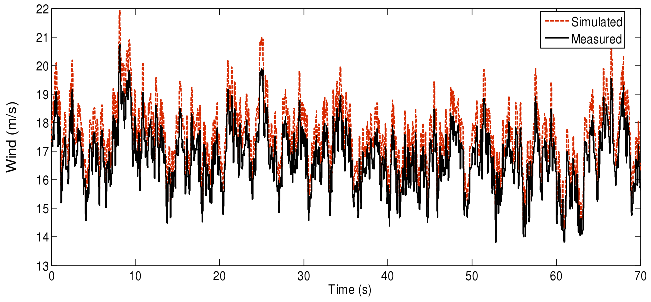

Fig. 10. Simulated high turbulence wind flow used in the study.

considered is 17 m/s. The response obtained by the DFIG-WPGS with the hybrid RBFNN-MPSO based MPPT controller and hybrid ENN-MPSO based MPPT controller for turbulence wind speeds has been depicted in Fig. 11.

Fig. 11(a) depicts the DFIG's rotor speed. The result specifies a slower dynamic variation of the rotor speed in RBFNN-MPSO based MPPT when compared to ENN-MPSO based MPPT. Fig. 11(b) depicts the tip speed ratio of the WPGS and it can be observed that the proposed RBFNN-MPSO based MPPT maintains an average optimal tip speed ratio of $\lambda_{opt} = 6.8$ Whereas, ENN-MPSO MPPT strategy maintains an average $\lambda = 6.67$. The corresponding power coefficient obtained is depicted in Fig. 11(c). The RBFNN-MPSO based MPPT strategy tracks an optimal power of 0.478 with a less oscillation than that of ENN-MPSO MPPT strategy. The turbine mechanical torque and DFIG electromagnetic torque is depicted in Fig. 11(d) and (e) and it is inferred that both strategies have an effective interaction with the rotor torque. Fig. 11(f) depicts a MPPT curve plotted between λ and C_p and it can be observed that the proposed RBFNN-MPSO based MPPT strategy achieves maximum power co-efficient of 0.475 and ENN-MPSO based MPPT strategy achieves power coefficient of 0.465 at optimal tip speed ratio, $\lambda = 6.89$ (avg.). The optimal power obtained in RBFNN-MPSO based MPPT strategy is 1% higher when compared to ENN-MPSO MPPT strategy. Fig. 12 shows the real

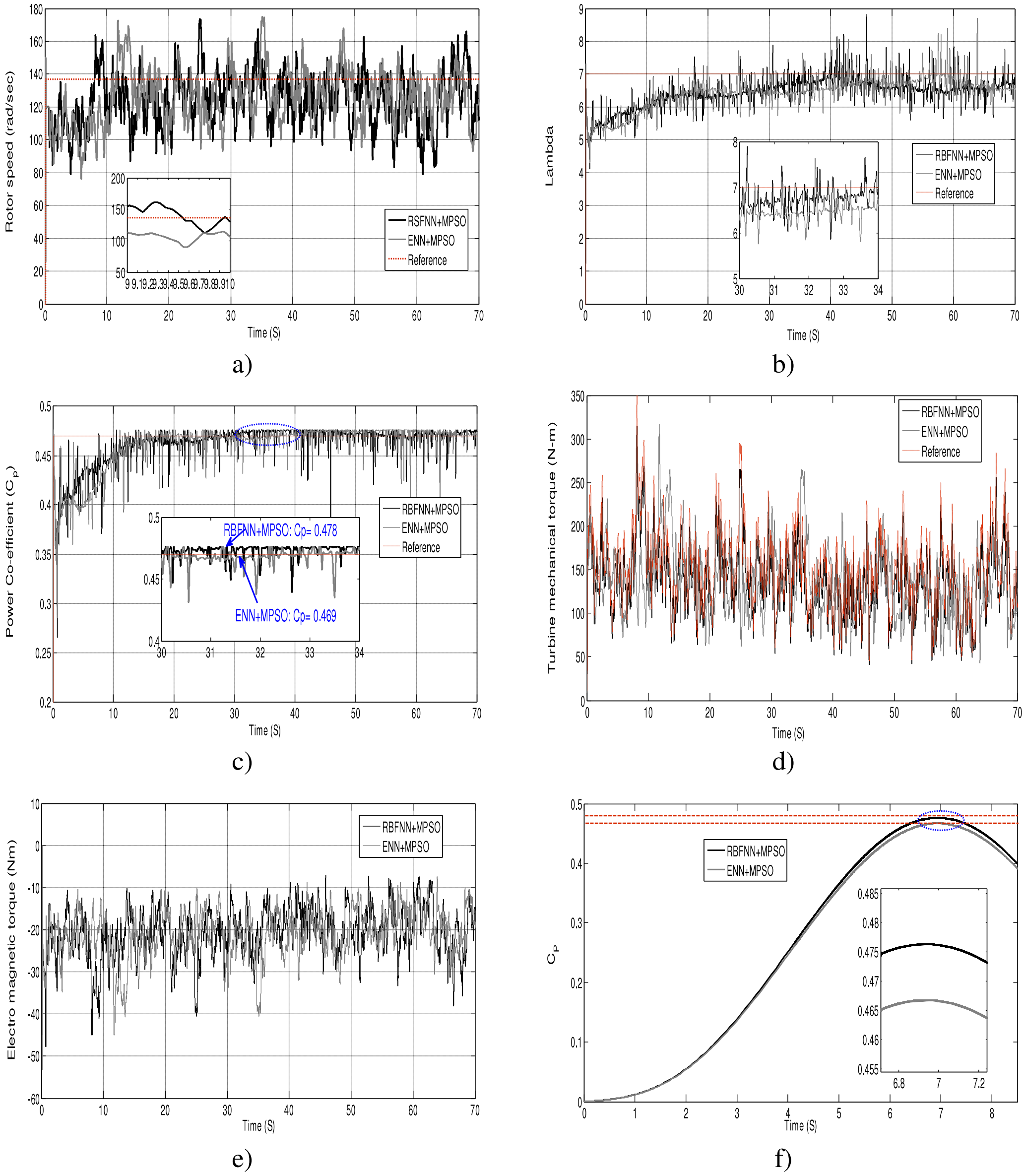

a)

b)

c)

d)

e)

f)

Fig. 11. Obtained response of the DFIG-WPGS with MPPT controller for high wind speed 14 m/s to 22 m/s. (a) Rotor speed (ω_r); (b) Tip speed ratio (λ-*Lambda*); (c) Power co-efficient (C_p); (d) Mechanical torque (T_m); (e) Electromagnetic toque (T_e); (f) MPPT-curve (λ *Vs* C_p).

Please cite this article as: R. Sitharthan, M. Karthikeyan, D.S. Sundar et al., Adaptive hybrid intelligent MPPT controller to approximate effectual wind speed and optimal rotor speed of variable speed wind turbine. ISA Transactions (2019), https://doi.org/10.1016/j.isatra.2019.05.029.

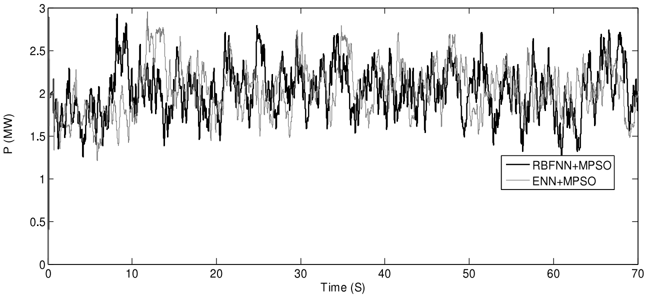

Fig. 12. Measured real power of DFIG-WPGS.

power obtained by DFIG-WPGS for 14 m/s to 22 m/s wind speeds. Figs. 9 and 12 illustrates that the power converter is equalized without altering the output power. This can dramatically reduce both cost and maintenance of overall system through minimizing the size of converters.

5.3. Comparison of different observation on control strategy

The performance comparison of various control strategy of TSR MPPT methodology has been tabulated in Table 1. From the tabulation it can be observed that the proposed control strategy has a minimized computation timing with enhanced power co-efficient. Furthermore, the power extraction efficiency of the proposed control strategy is 81% to 84% for various wind conditions. The obtained results are comparatively higher than the other studied control strategy. Further, the proposed MPPT control strategy has been compared with the reference [20,22,25], and [26] and are tabulated in Table 2. From the observation the proposed controller performs equally in all aspects with respect to the previous literature [20]. But the power co-efficient obtained is 1% higher than [20]. Therefore, the simulation analysis proves the successfulness of the proposed RBFNN-MPSO based MPPT control strategy for the DFIG based WPGS.

5.4. Experimental validation

The experimental setup has been built in the laboratory. The induction motor is assumed to be turbine simulator and is working in torque control mode. The electric motor is coupled with the induction generator as shown in Fig. 13. Both motors are energized through DSPACE-1103 environment. The experimental work is successfully carried out and it gives encouraging results for wind motor speed management, which commands the microcontroller and Simulink interface with serial communication. The control strategy is proposed to minimize the memory utilization of microcontroller and the compatibility of the proposed control strategy. The obtained results are depicted in Fig. 14. Fig. 14(a) shows the PWM modulation duty cycle obtained through RBFNN-MPSO control strategy which is given as triggering pulse for VSC. The PWM is purely estimated by SVPWM modulation based on the speed of the motor and estimated power with periodic switching frequency of 100 kHz. Fig. 14(b) shows the voltage and current obtained at no load condition. The V_0 is taken as 20 V/div and I_0 is taken as 0.1 mA/div. Fig. 14(c) depicts the voltage and current obtained at loaded condition. The V_1 is taken as 20 V/div and I_1 is taken as 3 A/div. The corresponding power is depicted in Fig. 14(d). Where the power P_1 is taken as $P_1 = V_1 x\, I_1$ at unity power factor. The obtained results show enhanced operation of the proposed control strategy.

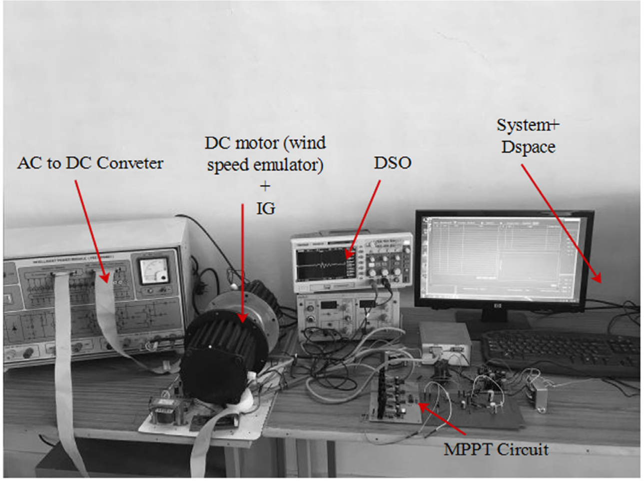

Fig. 13. Experimental setup.

6. Conclusion

A novel and intelligent MPPT control strategy for DFIG-WPGS is proposed in this research work. The proposed MPPT controller has an ability to govern the variable speed wind turbine system and track maximum power over a wide range of wind speeds. The proposed RBFNN-MPSO based MPPT controller performance is evaluated and a comparative analysis has been carried out with references. During analysis, following observations are enumerated to prove the performance of the proposed MPPT control strategy.

i. The obtained result shows that the proposed hybrid intelligent MPPT controller has an efficiency of 84% and has a very good accuracy when compared to its competitive MPPT control techniques.
ii. From analysis the proposed RBFNN-MPSO based MPPT controller reduces the speed variation range of DFIG-WPGS by effective tracking, thereby leading to rationalize the back to back converter pulse width modulation, and increases the reliability with fewer converter losses.

Therefore, the analysis proves that the proposed hybrid RBFNN-MPSO based MPPT controller has better efficiency and improved reliability in tracking maximum available power from wind.

Acknowledgement

This research received funding from the Science and Engineering Research Board, India, Department of Science & Technology, Government of India (ECR/2017/000259).

Declaration of competing interest

The authors declare that they have no known competing financial interests or personal relationships that could have appeared to influence the work reported in this paper.

Please cite this article as: R. Sitharthan, M. Karthikeyan, D.S. Sundar et al., Adaptive hybrid intelligent MPPT controller to approximate effectual wind speed and optimal rotor speed of variable speed wind turbine. ISA Transactions (2019), https://doi.org/10.1016/j.isatra.2019.05.029.

Table 1
Performance comparison with other MPPT controller.

Controller	Measured data					
	Wind speed	Iterative number	MSE	Computation time (s)	Measured power co-efficient	Power extraction efficiency %
RBFNN-MPSO	5 m/s to 12 m/s	148	1.235×10^{-3}	0.61	0.498	84
ENN-MPSO		167	1.414×10^{-3}	0.75	0.476	80.3
RBFNN-GA		163	1.334×10^{-3}	0.73	0.47	80
RBFNN		838	2.341×10^{-3}	1.10	0.431	73
ENN		975	2.612×10^{-3}	1.16	0.430	72.6
PID		–	–	–	0.408	69
RBFNN-MPSO	14 m/s to 22 m/s	234	1.4×10^{-3}	0.69	0.478	81
ENN-MPSO		226	1.52×10^{-3}	0.7	0.465	0.79
RBFNN-GA		189	1.45×10^{-3}	0.7	0.426	0.72
RBFNN		746	2.3×10^{-3}	1.13	0.41	0.69
ENN		834	2.6×10^{-3}	1.25	0.41	0.69
PID		–	–	–	0.4	68

Table 2
Performance comparison with reference.

Parameter	Control strategy				
	Proposed RBFNN+MPSO based TSR MPPT strategy	Optimal torque control based MPPT [20]	Maximum electrical power tracker-based strategy [25]	Quadratic Boost Converter based MPPT [22]	Perturbation observation based nonlinear adaptive control [26]
C_p	0.49	0.48	0.46	0.46	0.41
Complexity	Simple	Average	High	High	Simple
Convergence speed	Fast	Fast	Medium	Medium	Depends

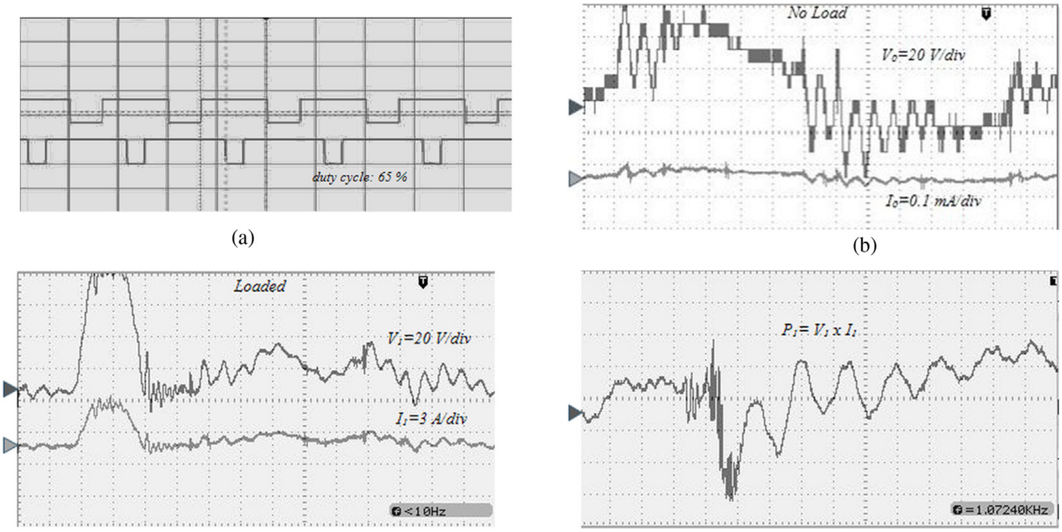

(a) (b) (c) (d)

Fig. 14. Experimental observation. (a) duty cycle; (b) *V-I* at no-load; (c) *V-I* at load; and (d) Power $P_1 = V_1 \; x \; I_1$ at load.

Appendix

The major study of this research is to identify the Parameters of the grid tied wind energy conversion system,

Wind turbine parameter: Mechanical output power, P_m = 2.5 MW; Tip speed ratio, λ = 7; Power-coefficient, Cp = 0.45.

DFIG parameter: Electrical output power, P_e = 2.5 MW; system frequency, f = 50 Hz; Lin-line voltage, V_L = 470 V; Stator resistance, R_s = 0.0229 p.u.; Stator leakage inductance, L_s = 0.171 p.u.; Rotor resistance, R_r = 0.0098 p.u., Rotor leakage inductance, L_r = 0.156 p.u.; Magnetizing inductance, L_m = 2.9 p.u.; Poles, p = 6; Friction factor, F = 0.01 p.u.;

Transmission line parameters: Grid filter impedance: $R_g + jX_g$ = 0.003 + j0.3 p.u.; Positive and zero sequence resistances: 0.1153, 0.413 X/km. Positive and zero sequence inductances: 1.05, 3.32 mH/km. Positive and zero sequence capacitances: 11.33, 5.01 μF/km. Sensitive linear load: 4.5 kVA

Transformer parameters: T1: 12 MVA, 470 V/20 KV, impedance: 0.0017 + j0.05 p.u.; T2: 47 MVA, 20 KV/120 KV, impedance: 0.00534 + j0.16 p.u.; Network impedance: Re + jXe = 0.0004 + j0.004 p.u.

References

[1] Painuly JP. Barriers to renewable energy penetration; a framework for analysis. Renew Energy 2001;24(1):73–89.

[2] Xiong P, Jirutitijaroen P, Singh C. A distributionally robust optimization model for unit commitment considering uncertain wind power generation. IEEE Trans Power Syst 2017;31(1):39–49.

[3] Sitharthan R, Swaminathan JN, Parthasarathy T. Exploration of wind energy in India: A short review. In: 2018 national power engineering conference (NPEC). IEEE; 2018, p. 1–5.

Please cite this article as: R. Sitharthan, M. Karthikeyan, D.S. Sundar et al., Adaptive hybrid intelligent MPPT controller to approximate effectual wind speed and optimal rotor speed of variable speed wind turbine. ISA Transactions (2019), https://doi.org/10.1016/j.isatra.2019.05.029.

[4] Sitharthan R, Geethanjali M. Application of the superconducting fault current limiter strategy to improve the fault ride-through capability of a doubly-fed induction generator–based wind energy conversion system. Simulation 2015;91(12):1081–7.

[5] Saravanakumar R, Jena D. Validation of an integral sliding mode control for optimal control of a three blade variable speed variable pitch wind turbine. Int J Electr Power Energy Syst 2015;69(1):421–9.

[6] Farbood M, Taherian-Fard E, Shasadeghi M, Izadian A, Niknam T. Dynamics and control of a shared wind turbine drivetrain. IEEE Trans Ind Appl 2018;54(6):6394–400.

[7] Bounar N, Labdai S, Boulkroune A. PSO–GSA based fuzzy sliding mode controller for DFIG-based wind turbine. ISA Trans 2019;85:177–88.

[8] Mokhtari Y, Rekioua D. High performance of maximum power point tracking using ant colony algorithm in wind turbine. Renew Energy 2018;126:1055–63.

[9] Kumar D, Chatterjee K. A review of conventional and advanced MPPT algorithms for wind energy systems. Renew Sustain Energy Rev 2016;55(1):957–70.

[10] Karabacak M. A new perturb and observe based higher order sliding mode MPPT control of wind turbines eliminating the rotor inertial effect. Renew Energy 2019;133:807–27.

[11] Ghaffari A, Krstic M, Seshagiri S. Power optimization and control in wind energy conversion systems using extremum seeking. IEEE Trans Control Syst Technol 2014;22(5):1684–95.

[12] Mousa MG, Allam SM, Rashad EM. Maximum power extraction under different vector-control schemes and grid-synchronization strategy of a wind-driven Brushless Doubly-Fed Reluctance Generator. ISA Trans 2018;1(72):287–97.

[13] de Matos JG, Silva FS, Ribeiro LA. Power control in ac isolated microgrids with renewable energy sources and energy storage systems. IEEE Trans Ind Electron 2015;62(6):3490–8.

[14] Ganjefar S, Ghassemi AA, Ahmadi MM. Improving efficiency of two-type maximum power point tracking methods of tip-speed ratio and optimum torque in wind turbine system using a quantum neural network. 2014;67(1):444–53.

[15] Parker CM, Leftwich MC. The effect of tip speed ratio on a vertical axis wind turbine at high Reynolds numbers. Exp Fluids 2016;57(5):74–84.

[16] Nasiri M, Milimonfared J, Fathi SH. Modeling, analysis and comparison of TSR and OTC methods for MPPT and power smoothing in permanent magnet synchronous generator-based wind turbines. Energy Convers Manage 2014;86(1):892–900.

[17] Lalouni S, Rekioua D, Idjdarene K, Tounzi A. Maximum power point tracking based hybrid hill-climb search method applied to wind energy conversion system. Electr Power Compon Syst 2015;43(10):1028–38.

[18] Cheng M, Zhu Y. The state of the art of wind energy conversion systems and technologies: A review. Energy Convers Manage 2014;88(1):332–47.

[19] Abdullah MA, Yatim AHM, Tan CW, Saidur R. A review of maximum power point tracking algorithms for wind energy systems. Renew Sustain Energy Rev 2012;16(5):3220–7.

[20] Asgharnia A, Shahnazi R, Jamali A. Performance and robustness of optimal fractional fuzzy PID controllers for pitch control of a wind turbine using chaotic optimization algorithms. ISA Trans 2018;79:27–44.

[21] Fathabadi H. Novel maximum electrical and mechanical power tracking controllers for wind energy conversion systems. IEEE J Emerg Sel Top Power Electron 2017;5(4):1739–45.

[22] Chen J, Yao W, Zhang CK, Ren Y, Jiang L. Design of robust MPPT controller for grid-connected PMSG-Based wind turbine via perturbation observation based nonlinear adaptive control. Renew Energy 2019;134:478–95.

[23] Sitharthan R, Devabalaji KR, Jees A. An Levenberg–Marquardt trained feed-forward back-propagation based intelligent pitch angle controller for wind generation system. Renew Energy Focus 2017;22:24–32.

[24] Tiwari R, Krishnamurthy K, Neelakandan RB, Padmanaban S, Wheeler PW. Neural network based maximum power point tracking control with quadratic boost converter for PMSG—Wind energy conversion system. Electronics 2018;7(2):20–6.

[25] Wang G, Wang J, Zhou Z, Wang Q, Wu Q, Jiang X, Santana E. State variable technique islanding detection using time-frequency energy analysis for DFIG wind turbine in microgrid system. ISA Trans 2018;80:360–70.

[26] Sitharthan R, Geethanjali M. An adaptive Elman neural network with C-PSO learning algorithm based pitch angle controller for DFIG based WECS. J Vib Control 2017;23(5):716–30.

[27] Addeh A, Khormali A, Golilarz NA. Control chart pattern recognition using RBF neural network with new training algorithm and practical features. ISA Trans 2018;79:202–16.

[28] Wang G, Wang J, Zhou Z, Wang Q, Wu Q, Jiang X, Santana E. State variable technique islanding detection using time-frequency energy analysis for DFIG wind turbine in microgrid system. ISA Trans 2018;80:360–70.

[29] de Leon-Delgado H, Praga-Alejo RJ, Gonzalez-Gonzalez DS, Cantú-Sifuentes M. Multivariate statistical inference in a radial basis function neural network. Expert Syst Appl 2018;1(93):313–21.

[30] Stogiannos M, Alexandridis A, Sarimveis H. Model predictive control for systems with fast dynamics using inverse neural models. ISA Trans 2018;1(72):161–77.

[31] Karthikeyan M, Saraswady D. Low complexity layered tabu search detection in large MIMO systems. AEU-Int J Electron Commun 2018;83:106–13.

[32] Rezk H, Fathy A, Abdelaziz AY. A comparison of different global MPPT techniques based on meta-heuristic algorithms for photovoltaic system subjected to partial shading conditions. Renew Sustain Energy Rev 2017;74(1):377–86.

[33] Sitharthan R, Parthasarathy T, Sheeba Rani S, Ramya KC. An improved radial basis function neural network control strategy-based maximum power point tracking controller for wind power generation system. Trans Inst Meas Control 2019;0142331218823858.

[34] Sitharthan R, Sundarabalan CK, Devabalaji KR, Yuvaraj T, Mohamed Imran A. Automated power management strategy for wind power generation system using pitch angle controller. Meas Control 2019. p.0020294019827330.

[35] Sitharthan R, Sundarabalan CK, Devabalaji KR, Nataraj SK, Karthikeyan M. Improved fault ride through capability of DFIG-wind turbines using customized dynamic voltage restorer. Sustainable Cities Soc 2018;39:114–25.

[36] Kumar P, Bhowmick B. 2d analytical model for surface potential based electric field and impact of wok function in DMG SB MOSFET. Superlattices Microstruct 2017;109:805–14.

[37] Mousa MG, Allam SM, Rashad EM. Maximum power extraction under different vector-control schemes and grid-synchronization strategy of a wind-driven brushless doubly-fed reluctance generator. ISA Trans 2018;72:287–97.

[38] Kumar P, Bhowmick B. Suppression of ambipolar conduction and investigation of RF performance characteristics of gate-drain underlap SiGe Schottky barrier field effect transistor. Micro Nano Lett 2018;13(5):626–30.

Please cite this article as: R. Sitharthan, M. Karthikeyan, D.S. Sundar et al., Adaptive hybrid intelligent MPPT controller to approximate effectual wind speed and optimal rotor speed of variable speed wind turbine. ISA Transactions (2019), https://doi.org/10.1016/j.isatra.2019.05.029.